SUPPLEMENTARY METHODS

RNA *in situ* hybridization

Deletion of *Fgfr2* from cre-expressing regions was validated by *in situ* hybridization using a digoxigenin-labeled antisense riboprobe synthesized from linearized plasmid containing exons 9–10 of *Fgfr2* (*Fgfr2iiic-TM*, kindly provided by D. Ornitz). *Fgfr2* expression in wildtype tissue was analyzed using a riboprobe recognizing the cytoplasmic tyrosine kinase domain of FGFR2 from linearized *Fgfr2TK* plasmid (De Moerlooze et al., 2000). Whole mount *in situ* hybridization was performed according to published methods (Nieto et al., 1996) with the exceptions that Triton X-100 was replaced with Tween-20 in KTBT solution and the concentration of Triton X-100 in NTMT solution was raised from 0.1% to 1%.

Experimental design

To minimize the effects of subtle stage variation among embryos within a single litter, each mutant embryo was compared to a stage-matched control littermate of the same sex. Except where noted, only data collected from male embryos was analyzed and reported. In experiments performed on tissue sections, at least 8 non-adjacent tissue sections were examined per embryo. Analysis of multiple cellular markers (e.g., cell adhesion, cytoskeletal, and cell cycle proteins) in individual genital tubercles was carried out using single antibodies on adjacent serial sections or using multiple antibodies for co-localization on single sections. Each figure in the manuscript is representative of the totality of data.

Table S1. Embryo collection and tissue fixation

Experiment	Embryonic or neonatal tissue processed	Dissection medium	Fixative	Fixation temperature, duration
X-Gal staining of β-galactosidase	Pelvis and posterior abdomen	PBS	0.2% PFA	4°C, overnight
Immunohistochemistry/ immunofluorescence	Pelvis and posterior abdomen, hindlimbs removed	PBS	0.2% PFA	4°C, overnight
Histology	Pelvis and posterior abdomen, hindlimbs removed	PBS	4% PFA	4°C, overnight
Scanning electron microscopy	Genital tubercle with ventral body wall and proximal tail	PBS	1% GA/4% PFA	4°C, overnight
Transmission electron microscopy	Genital tubercle with ventral body wall	PBS	1% GA/4% PFA in sodium cacodylate	4°C, overnight
Whole mount *in situ* hybridization	Pelvis and posterior abdomen	DEPC PBS	4% PFA	4°C, overnight
Quantitative real-time PCR	Genital tubercle	DEPC PBS	RNAlater (Qiagen)	–20°C, indefinite

Table S2. Analyses performed on tissue sections

Protocol	Preparation and infiltration	Embedding medium	Stain
Histology	Dehydrated to absolute ethanol, permeabilized with Xylene	Paraffin (1:1 Paraplast Xtra and Plus)	Masson's trichrome (Richard Allan Scientific)
Histology on X-Gal stained tissue	Dehydrated to absolute ethanol, permeabilized with Xylene	Paraffin (1:1 Paraplast Xtra and Plus)	Nuclear fast red or Harris' Hematoxylin and 1% Eosin Y
Immunohistochemistry	Dehydrated to absolute ethanol, permeabilized with Xylene	Paraffin (1:1 Paraplast Xtra and Plus)	--
Immunofluorescence	Equilibrated with 30% sucrose	OCT (Tissue-Tek)	--
Transmission electron microscopy	Dehydrated to pure acetone, resin infiltrated in graded acetone/Spurrs epoxy resin (Ellis, 2006)	Spurrs epoxy resin	2% Uranyl acetate and Reynold's lead citrate

Table S3. Antibodies

Primary antibody	Clone or catalog number	Manufacturer	Secondary antibody	Clone or catalog number	Manufacturer
Mouse IgG_3 anti-cytokeratin14	NCL-LL002	Novacastra	Goat anti-mouse IgG, HRP conjugate	P 0447	Dako
Rabbit IgG anti-Fgfr2 (Bek)	C-17	Santa Cruz	AlexaFluor-647 goat anti-rabbit IgG	A-21244	Molecular Probes
Mouse IgG_1 anti-βcatenin	14	BD Biosciences	AlexaFluor-546 goat anti-mouse IgG_1	A-21123	Molecular Probes
Rabbit IgG anti-phospho-Histone H3	06-570	Millipore	AlexaFluor-488 goat anti-rabbit IgG	A-11008	Molecular Probes
Mouse IgG_1 anti-BrdU	G3G4	Developmental Studies Hybridoma Bank	AlexaFluor-546 goat anti-mouse IgG_1	A-21123	Molecular Probes

Table S4. Primer sequences

Primer	Type	Sequence
smcx1	Genotyping	5′-CCG-CTG-CCA-AAT-TCT-TTG-G
smc4	Genotyping	5′-TGA-AGC-TTT-TGG-CTT-TGA-G
Cre forward	Genotyping	5′-TGA-CGG-TGG-GAG-AAT-GTT-AAT
Cre reverse	Genotyping	5′-GCC-GTA-AAT-CAA-TCG-ATG-AGT
$Fgfr2^{flox}$ forward	Genotyping	5′-ATA-GGA-GCA-ACA-GGC-GG
$Fgfr2^{flox}$ reverse	Genotyping	5′-TGC-AAG-AGG-CGA-CCA-GTC-AG
Shh^{C} forward	Genotyping	5′-ATG-CTG-GCT-CGC-CTG-GCT-GTG-GAA
Shh^{C} reverse	Genotyping	5′-GAA-GAG-ATC-AAG-GCA-AGC-TCT-GGC
Rosa forward	Genotyping	5′-AAA-GTC-GCT-CTG-AGT-TGT-TAT
Rosa reverse	Genotyping	5′-GGA-GCG-GGA-GAA-ATG-GAT-ATG
LacZ reverse	Genotyping	5′-GCG-AAG-AGT-TTG-TCC-TCA-ACC
βcatenin forward	qRT-PCR	5′-GTG-CAA-TTC-CTG-AGC-TGA-CA
βcatenin reverse	qRT-PCT	5′-CTT-AAA-GAT-GGC-CAG-CAA-GC
Fgfr2 forward	qRT-PCR	5′-TCT-GGG-ACC-TCC-TTC-CAT-CTT-CTT
Fgfr2 reverse	qRT-PCR	5′-ACT-GTA-GCA-AAG-TGA-GTG-GGC-GTA
GAPDH forward	qRT-PCR	5′-CCA-AGG-TCA-TCC-ATG-ACA-ACT
GAPDH reverse	qRT-PCR	5′-ATC-ACG-CCA-CAG-CTT-TCC
Ptch1 forward	qRT-PCR	5′-TTG-TGG-AAG-CCA-CAG-AAA-ACC
Ptch1 reverse	qRT-PCR	5′-TGT-CTG-GCG-TCC-GGA-TGG-A
Shh forward	qRT-PCR	5′-ACG-GAC-CTT-CAA-GAG-CCT-TA
Shh reverse	qRT-PCR	5′-CCC-ATG-GAG-CAG-GTT-TTA-GT

SUPPLEMENTARY REFERENCES

De Moerlooze, L., Spencer-Dene, B., Revest, J.-M., Hajihosseini, M., Rosewell, I. and Dickson, C. (2000). An important role for the IIIb isoform of fibroblast growth factor receptor 2 (FGFR2) in mesenchymal-epithelial signalling during mouse organogenesis. *Development* **127**, 483-492.

Nieto, M. A., Patel, K. and Wilkinson, D. G. (1996). *In situ* hybridization analysis of chick embryos in whole mount and tissue sections. *Method Cell Biol*. **51**, 219-235.

Petiot, A., Perriton, C. L., Dickson, C. and Cohn, M. J. (2005). Development of the mammalian urethra is controlled by Fgfr2-IIIb. *Development* **132**, 2441-2450.

SUPPLEMENTARY FIGURE LEGENDS

Figure S1. Conditional inactivation of *Fgfr2* in the urethral and surface epithelia of the genital tubercle. (**A-D**) *Fgfr2* expression in the developing external genitalia (Petiot et al., 2005) was validated by *in situ* hybridization on E13.5 whole genital tubercles (A,B) and transverse sections (C,D) using an antisense riboprobe complementary to the cytoplasmic tyrosine kinase (TK) domain of *Fgfr2* (*Fgfr2TK;* De Moerlooze et al., 2000). *Fgfr2* transcription was detected on the genital tubercle surface epithelium, including the preputial swellings (arrowheads), and in the developing urethra (arrow). (C,D) In tissue sections, *Fgfr2* expression was detected in the developing corpora cavernosa (cc), preputial glands (pg), urethra, and surface epithelium. In epithelia, *Fgfr2TK* transcript was most abundant in basal layers (triangle), although mRNA was also detected in suprabasal cells (D). (**E-J'**) Deletion of *Fgfr2* from target tissues was verified by whole mount *in situ* hybridization using an RNA probe specific to the floxed region of *Fgfr2*. Expression of both *Fgfr2* isoforms was visualized; the $Fgfr2^{flox}$ loxP sites flank exons 7 (IIIa), 8 (IIIb), and 9 (IIIc) (Yu et al., 2003), and the *Fgfr2iiic-TM* riboprobe hybridizes to exons 9 and 10

(transmembrane, TM). At E12.5 *Fgfr2* expression is evident in the distal urethra (arrows) of control and $Fgfr2^{Ecto\Delta}$ mutant genital tubercles but is absent from $Fgfr2^{Endo\Delta}$ mutants. By E14.5, *Fgfr2* transcripts are detectable in the urethral and surface ectodermal (arrowheads) epithelia of controls, but are absent from the urethrae of $Fgfr2^{Endo\Delta}$ mutants and from the surface ectoderm of $Fgfr2^{Ecto\Delta}$ mutants. Restriction of *Fgfr2* expression to Cre-negative regions of the genital tubercles confirms that *Fgfr2* is deleted specifically in the cells targeted by the Cre alleles. (**K-M**) Immunofluorescence of FGFR2 reveals no changes in the localization of ectodermal FGFR2 in $Fgfr2^{Endo\Delta}$ mutants, of urethral FGFR2 in $Fgfr2^{Ecto\Delta}$ mutants, or of mesenchymal FGFR2 (yellow arrows) in either mutant. Scale bars: 100 μm.

Figure S2. Variation in hypospadias and preputial anomalies resulting from ectodermal *Fgfr2* deletion. Oversized and ectopic urethral openings in $Fgfr2^{Ecto\Delta}$ mutants at P0 can be seen in β-galactosidase-stained male (**A-D**) and female (**E**), and in unstained female (**F**) genital tubercles. Urethral tube defects range in severity from glanular (A), to coronal (B), to midshaft (C), to proximal (D) hypospadias in males. Female mutants also develop hypospadias (E,F). Arrows denote urethral meatuses; arrowheads mark preputial ectoderm. Scale bars: 100 μm.

Figure S3. Urethral cells lacking *Fgfr2* do not undergo epithelial-mesenchymal transition. Immunohistochemical analysis of K14 in transverse sections of β-galactosidase-stained $Fgfr2^{Endo\Delta}$ and control genital tubercles at E14.5 shows that endodermal cells (blue) remain

within the urethral epithelium and are not detected in the adjacent mesenchyme. Scale bars: 50 μm.

Figure S4. Development of the genital tubercle in the absence of ectodermal *Fgfr2*. Light micrographs of *Fgfr2*$^{Ecto\Delta}$ mutant and control genital tubercles from stages E13 to E16 show that *Fgfr2*$^{Ecto\Delta}$ mutants develop an ectopic proximal urethral opening (insets in A-D) that expands into an abnormally large hypospadic opening (arrows in E,F). The preputial swellings are displaced dorsally at early stages (white triangles in A-D) and fail to meet at the ventral midline at later stages (black triangles in E,F). Scale bars: 100 μm.

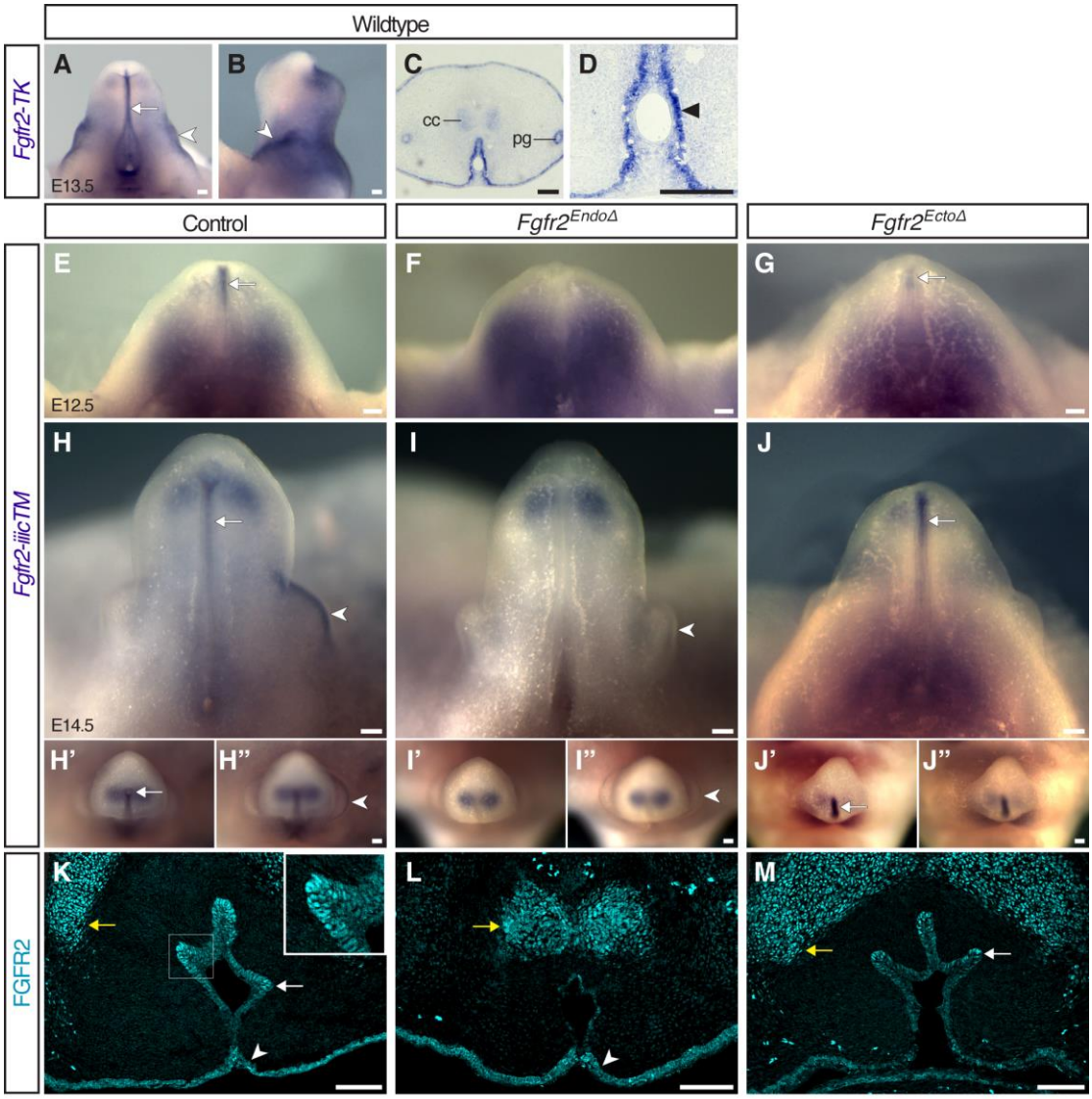

Figure S1. Conditional inactivation of *Fgfr2* in the urethral and surface epithelia of the genital tubercle.

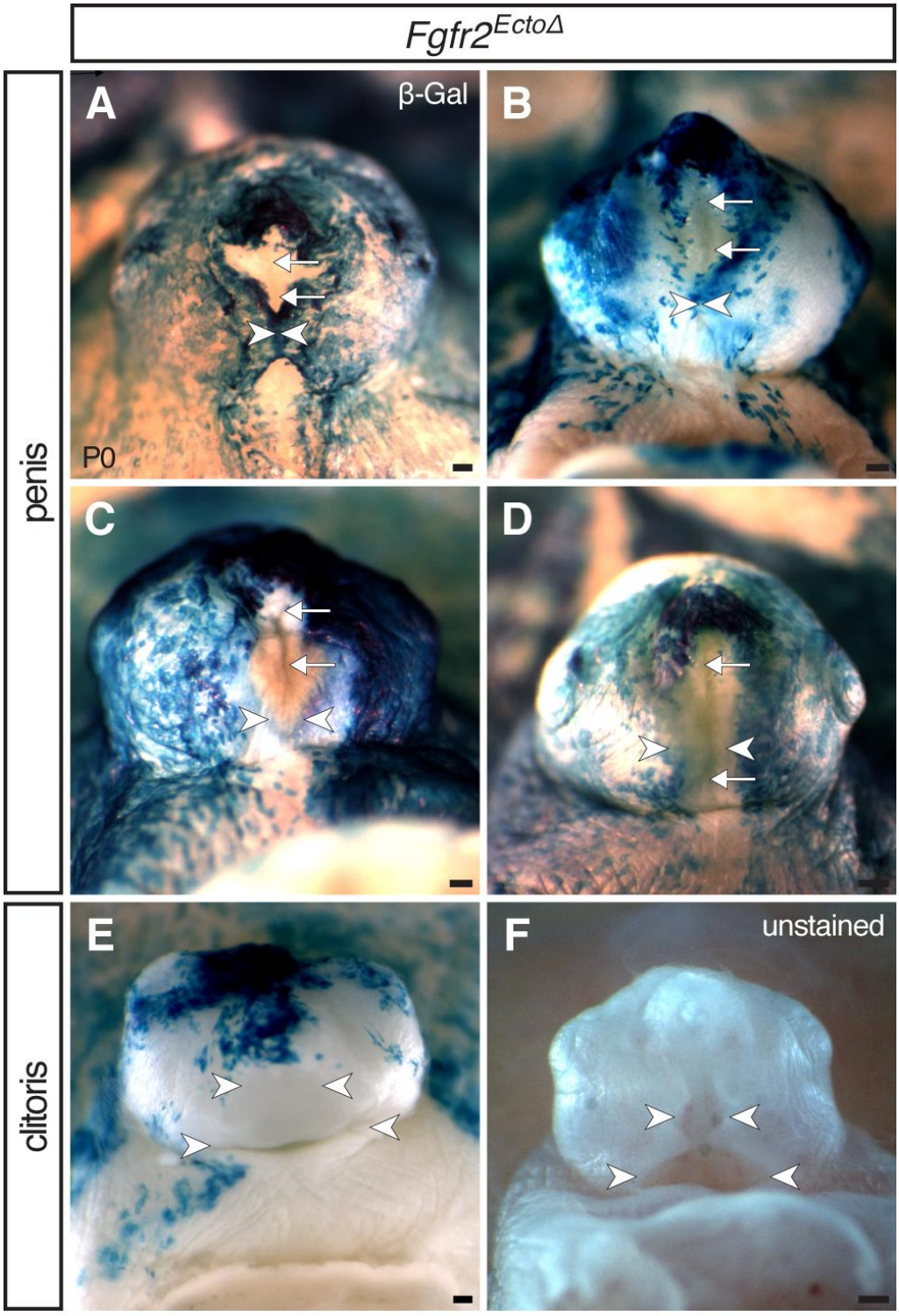

Figure S2. Variation in hypospadias and preputial anomalies resulting from ectodermal *Fgfr2* deletion.

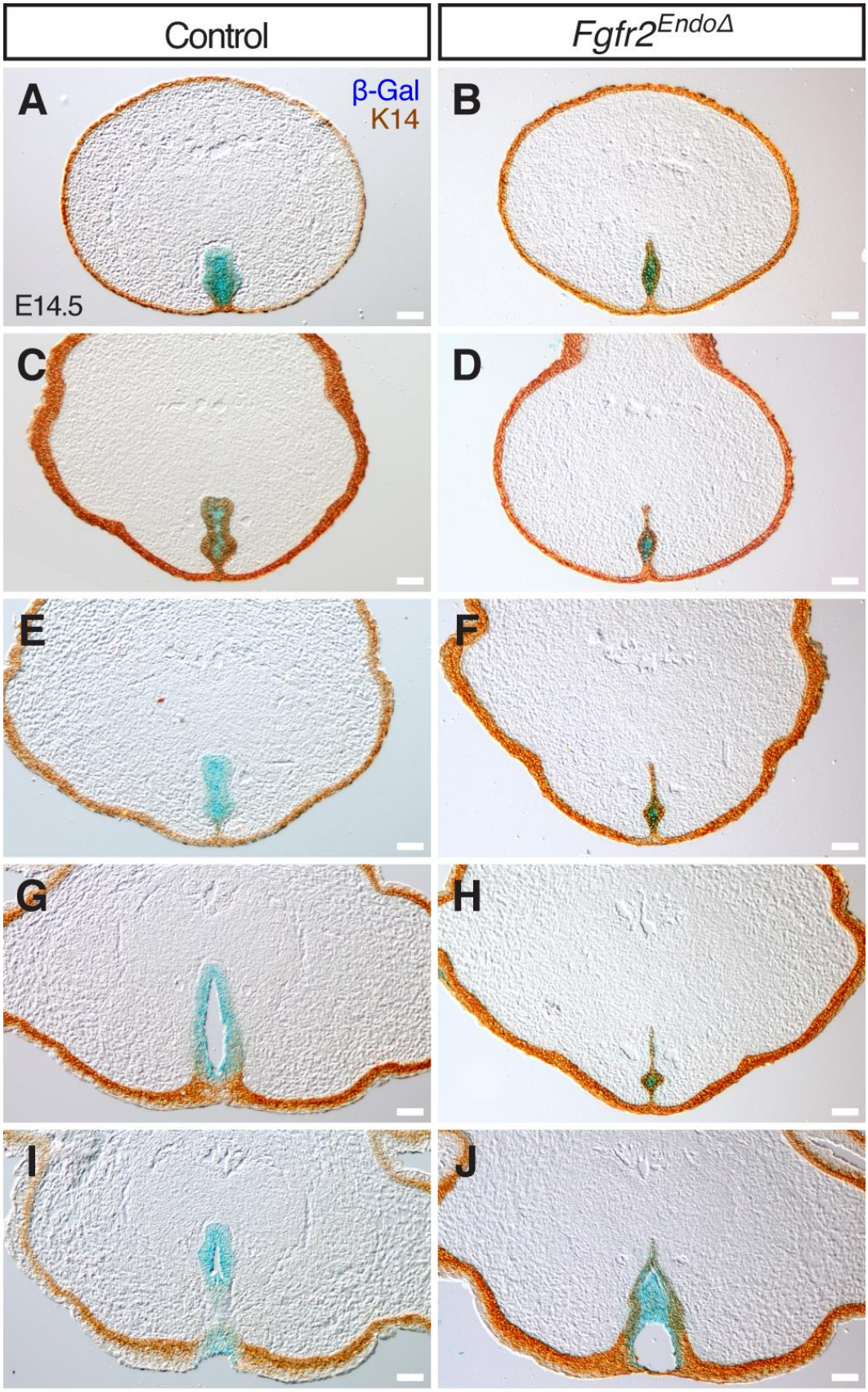

Figure S3. Urethral cells lacking *Fgfr2* do not undergo epithelial-mesenchymal transition.

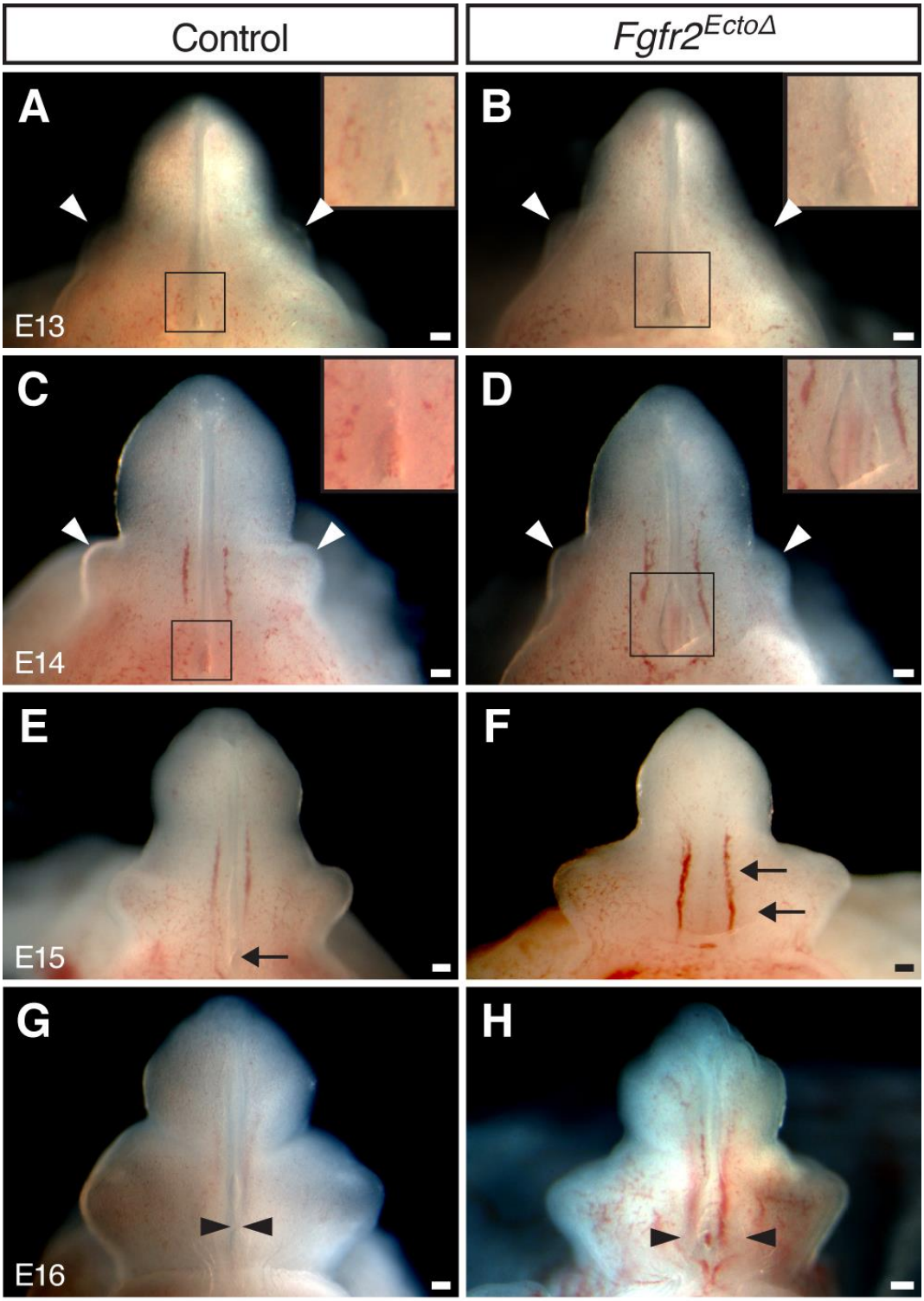

Figure S4. Development of the genital tubercle in the absence of ectodermal *Fgfr2*.